

Fast Multipole Method for Targets Above or Buried in Lossy Soil

N. Geng¹ and L. Carin²

¹Institut für Höchstfrequenztechnik und Elektronik,
Universität Karlsruhe, Kaiserstraße 12, D-76128 Karlsruhe, Germany

²Department of Electrical and Computer Engineering,
Duke University, Box 90291, Durham, NC 27708-0291

1. Introduction

The modeling of electromagnetic scattering has been of longstanding interest, with the method of moments (MoM) [1] representing a prominent example. While the MoM is powerful, it has limitations that restrict its utility. In particular, for N unknowns, the required memory (RAM) is of order $O(N^2)$, while the computational complexity depends on whether a direct (LU-decomposition) or iterative (conjugate gradient CG) solver is applied, the former requiring $O(N^3)$ operations and the latter $O(N^2)$ operations per iteration. To counter these limitations, there has been significant interest in the fast multipole method (FMM) [2-5]. The simplest two-level implementation [2,3] has complexity $O(N^{3/2})$ in RAM and CPU, while a multi-level FMM [4,5] further reduces this to $O(N \log N)$. While the FMM represents a promising tool, it has heretofore been applied primarily to free-space scattering [2-5], 2D analysis in layered media [6], or quasi-planar 3D problems in circuit and antenna design [7]. There are many important applications for which the free-space model or the quasi-planar approximation are not valid. For example, there has been significant interest in radar sensing of buried targets, such as mines or unexploded ordnance (UXO). Moreover, the soil must be included in the analysis of scattering from a target situated above and near the ground (*e.g.*, vehicles). While mines are generally small, and therefore amenable to an MoM analysis, many targets of interest are not. It is therefore desirable to adapt the FMM to the problem of scattering from a target in the vicinity of a half-space interface. Here we concentrate on an extension of the two-level FMM [2, 3], while similar modifications are possible with the multi-level FMM [4,5].

2. Half-space fast multipole method

We utilize the half-space electric field integral equation (EFIE) [1,8]

$$\hat{\mathbf{n}} \times \mathbf{E}^{inc}(\mathbf{x}) = \hat{\mathbf{n}} \times j\omega\mu_i \iint_{S'} \left[\bar{\mathbf{I}} + \frac{\nabla\nabla}{k_i^2} \right] \cdot \bar{\mathbf{G}}_{Aii}(\mathbf{x}, \mathbf{x}') \cdot \mathbf{J}(\mathbf{x}') dS' \quad (1)$$

for a general 3D PEC target situated entirely in layer $i=1$ or $i=2$ of a half space (Fig. 1). To avoid problems with interior resonances (for closed targets), a combined field integral equation (CFIE) [4] could be used instead. Details on the dyadic half-space Green's function can be found in [8]. Like in the MoM, the surface current $\mathbf{J}(\mathbf{x}')$ is expanded into a set of basis functions $\mathbf{b}_n(\mathbf{x}')$, where we use the RWG basis defined on flat triangles representing the surface [1]. Testing (1) with a set of weighting functions $\mathbf{w}_n(\mathbf{x})$ results in a system of N linear equations (*i.e.*, $[\mathbf{Z}] \cdot \mathbf{I} = \mathbf{V}$) for the current coefficients, with the matrix elements given by

$$Z_{nn'} = j\omega\mu_i \iint_S \iint_{S'} \mathbf{w}_n(\mathbf{x}) \cdot \left[\bar{\mathbf{I}} + \frac{\nabla\nabla}{k_i^2} \right] \cdot \bar{\mathbf{G}}_{Aii}(\mathbf{x}, \mathbf{x}') \cdot \mathbf{b}_{n'}(\mathbf{x}') dS' dS \quad (2)$$

In the FMM [2,3], we divide the computation into "near" and "far" terms. For 0-7803-5639-X/99/\$10.00 © 1999 IEEE.

“near” interactions (*i.e.*, MoM part of FMM) we evaluate the half-space Green’s function using the method of complex images [9]. Matrix elements representing “near” terms are stored in a sparse matrix [Z^{near}]. For “far” terms we split the dyadic into a “direct” contribution (as in free space, but general *complex* wavenumber k_i) and a remaining dyadic accounting for the interface (Δ is *not* an operator)

$$\tilde{\mathbf{G}}_{Aii}(\mathbf{x}, \mathbf{x}') = \tilde{\mathbf{I}}g_i(\mathbf{x}, \mathbf{x}') + \Delta\tilde{\mathbf{G}}_{Aii}(\mathbf{x}, \mathbf{x}') = \tilde{\mathbf{I}}\frac{e^{-jk_i|\mathbf{x}-\mathbf{x}'|}}{4\pi|\mathbf{x}-\mathbf{x}'|} + \Delta\tilde{\mathbf{G}}_{Aii}(\mathbf{x}, \mathbf{x}') \quad (3)$$

Consequently, the impedance matrix elements in (2) are split according to

$$\mathbf{Z}_{nn'} = \mathbf{Z}_{nn'}^{near} + \mathbf{Z}_{nn'}^{far} = \mathbf{Z}_{nn'}^{near} + \mathbf{Z}_{nn'}^{far,hom} + \Delta\mathbf{Z}_{nn'}^{far} \quad (4)$$

Using the addition theorem and a plane wave decomposition of the scalar free-space Green’s function, the “far” matrix elements in the 3D *free-space* FMM are written as [2,3] (for a definition of the geometrical parameters see Fig. 1)

$$\mathbf{Z}_{nn'}^{far,hom} = \frac{\omega\mu_0 k_i}{(4\pi)^2} \iint_{4\pi} \mathbf{W}_{m\alpha}(\hat{\mathbf{k}}) \cdot T_L(k_i X_{m'm}, \hat{\mathbf{k}} \cdot \hat{\mathbf{X}}_{m'm}) \mathbf{B}_{m'\alpha'}(\hat{\mathbf{k}}) d^2\hat{\mathbf{k}} \quad (5a)$$

$$\mathbf{W}_{m\alpha}(\hat{\mathbf{k}}) = [\tilde{\mathbf{I}} - \hat{\mathbf{k}}\hat{\mathbf{k}}] \cdot \iint_S \mathbf{w}_{n(m,\alpha)}(\mathbf{x}) e^{-jk_i\hat{\mathbf{k}}\cdot(\mathbf{x}-\mathbf{x}_m)} dS \quad (5b)$$

$$\mathbf{B}_{m'\alpha'}(\hat{\mathbf{k}}) = [\tilde{\mathbf{I}} - \hat{\mathbf{k}}\hat{\mathbf{k}}] \cdot \iint_{S'} \mathbf{b}_{n'(m',\alpha')}(\mathbf{x}') e^{+jk_i\hat{\mathbf{k}}\cdot(\mathbf{x}'-\mathbf{x}_{m'})} dS' \quad (5c)$$

$$T_L(k_i X_{m'm}, \hat{\mathbf{k}} \cdot \hat{\mathbf{X}}_{m'm}) = \sum_{l=0}^L (-j)^l (2l+1) h_l^{(2)}(k_i X_{m'm}) P_l(\hat{\mathbf{k}} \cdot \hat{\mathbf{X}}_{m'm}) \quad (5d)$$

In case of Galerkin testing and a lossless medium, (5b,5c) are complex-conjugate pairs. Consequently, either (5b) or (5c) need be stored in memory [2,3]. However, here we are interested in a general lossy half space (*i.e.*, k_i is *complex*), and therefore both must be computed. For an application of (5), the scatterer surface is first partitioned into groups $m=1, \dots, M$, each of which has an average number of $A_m \approx N/M$ basis functions. Inside group m the elements are labeled as $\alpha=1 \dots A_m$. The group information $n(m,\alpha)$ is stored in matrix format. As was shown in [2,3] for the two-level FMM, the optimal number of groups is $M \sim N^{1/2}$. Empirical approximations for the number L of terms needed in (5d) are given in [2,3,5] for a real wavenumber k_i . For complex k_i more terms are required [10]. Therefore, in our implementation L is determined adaptively at the beginning.

Using (5), the complexity with respect to RAM and CPU (for performing matrix-vector multiplies in the CG solver) is reduced from N^2 to $N^{3/2}$ [2,3]. The basic steps described in [2,3] remain valid to account for [Z^{near}] and the “direct” part [$Z^{far,hom}$] of the “far” interactions (see also final algorithm below).

However, for the half-space it is essential to include the “far” interface interactions represented by [ΔZ^{far}] in (4). The method of complex images [9] represents the Green’s function components as sums of free-space Green’s functions (with sources in complex space), which can, in principle, be handled within the FMM. While addition theorem and plane wave expansion remain valid for a complex wavenumber and complex images, the convergence is considerably slower [10]. Therefore, we utilize an approximate but highly accurate method for evaluating

the “far” interface interactions. In particular, if the target is entirely above or below the interface, and if basis and testing functions are distant, the “reflected” term can be evaluated asymptotically [11], leading to an image in real space with the amplitude given by the polarization dependent reflection coefficient.

Generalizing the free-space FMM is now straightforward. In the preprocessing stage [2,3] we include additional calculations of the translation operator (5d) between *image* and observation group centers as well as the spectral Fourier transforms $\mathbf{B}_{m\alpha}^{(v)}(\hat{\mathbf{k}})$ of the *image* expansion functions [10]. Extending [2,3], the matrix-vector multiplies in the CG solution are performed according to

$$\mathbf{s}_m^{(v)}(\hat{\mathbf{k}}) = \sum_{\alpha'=1}^{A_{m'}} I_{n'(m',\alpha')} \mathbf{B}_{m'\alpha'}^{(v)}(\hat{\mathbf{k}}) \quad (6a)$$

$$\mathbf{g}_m(\hat{\mathbf{k}}) = \sum_{m'=1}^M T_L(k_i X_{m'm}, \dots) \mathbf{s}_{m'}(\hat{\mathbf{k}}) + T_L(k_i X_{m'm}^v, \dots) \tilde{\mathbf{F}}_{m'm}^v \cdot \mathbf{s}_{m'}^v(\hat{\mathbf{k}}) \quad (6b)$$

$$\sum_{n'=1}^N Z_{nn'} I_{n'} = \sum_{n'=1}^N Z_{nn'}^{near} I_{n'} + \frac{\omega \mu_i k_i}{(4\pi)^2} \iint_{4\pi} \mathbf{W}_{m\alpha}(\hat{\mathbf{k}}) \cdot \mathbf{g}_m(\hat{\mathbf{k}}) d^2 \hat{\mathbf{k}} \quad , \quad (6c)$$

where the summation in (6b) is over “far” interactions only. The first term in (6b) represents “direct” contributions, the reflection dyadic and translation operator in the second term account for “far” interface interactions [10]. The three steps in (6a)–(6c) are often called aggregation, translation and disaggregation [4], the basic physical interpretation remains unchanged here.

3. Results

We demonstrate the accuracy of the half-space FMM by considering two targets: a model UXO buried under soil (Fig. 2) and a rectangular box situated above the ground (Fig. 3). All relevant parameters can be found in the figure captions. In all examples, the *bistatic* RCS is computed via the FMM developed here, as well as with a rigorous MoM, wherein the half-space Green’s function is evaluated rigorously via the method of complex images [9]. Figs. 2 and 3 show an excellent agreement between FMM and MoM results, for co- and cross-polarized RCS. The RAM and CPU requirements of the half-space FMM are about twice to three times compared to the free-space FMM [10] (caused by the extra set of real images and the additional Fourier transforms (5b,5c), needed because (5b) and (5c) are no longer conjugate complex), but the complexity of $N^{3/2}$ is unchanged.

References

- [1] S.M. Rao, D.R. Wilton, A.W. Glisson, “Electromagnetic scattering from surfaces of arbitrary shape,” *IEEE Trans. AP*, vol. 30, pp. 409-418, May 1982
- [2] R. Coifman, V. Rokhlin, S. Wandzura, “The fast multipole method for the wave equation: a pedestrian prescription,” *IEEE Ant. Prop. Magazine*, vol. 35, pp. 7-12, June 1993
- [3] J.M. Song, W.C. Chew, “Fast multipole method solution using parametric geometry,” *Micr. Opt. Techn. Letters*, vol. 7, pp. 760-765, Nov. 1994
- [4] J.M. Song, W.C. Chew, “Multilevel fast multipole algorithm for solving combined field integral equations of electromagnetic scattering,” *Micr. Opt. Techn. Letters*, vol. 10, pp. 14-19, Sept. 1995
- [5] J.M. Song, C.C. Lu, W.C. Chew, “Multilevel fast multipole algorithm for electromagnetic scattering by large complex objects,” *IEEE Trans. AP*, pp. 1488-1493, Oct. 1997
- [6] L. Gürel, M.I. Aksun, “Electromagnetic scattering solution of conducting strips in layered media using the fast multipole method,” *IEEE Micr. Guided Wave Let.*, vol. 6, pp. 277-279, Aug. 1996

- [7] J.S. Zhao, W.C. Chew, C.C. Lu, E. Michielssen, and J. Song, "Thin-stratified medium fast-multipole algorithm for solving microstrip structures," *IEEE Trans. MTT*, vol. 46, pp. 395-403, Apr. 1998
- [8] K.A. Michalski, D. Zheng, "Electromagnetic scattering and radiation by surfaces of arbitrary shape in layered media," *IEEE Trans. AP*, vol. 38, pp. 335-352, March 1990
- [9] M.I. Aksun, "A robust approach for the derivation of closed-form Green's functions," *IEEE Trans. MTT*, vol. 44, pp. 651-658, May 1996
- [10] N. Geng, A. Sullivan, L. Carin, "Fast multipole method for scattering from an arbitrary PEC target above or buried in a lossy half space," submitted to *IEEE Trans. AP*
- [11] I.V. Lindell, *Methods for Electromagnetic Field Analysis*, IEEE Press, 1995

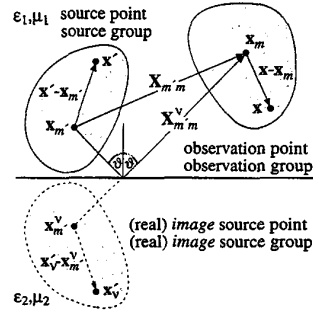


Fig. 1 Source, real image and observation group in 3D half-space FMM.

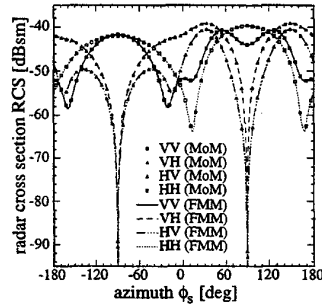


Fig. 2 RCS of a UXO (cylinder with spherical endcap, length=153cm, diameter=40.6cm) buried in Yuma soil with 5% water. The target axis lies in the yz-plane, 30° relative to the z-axis, with the nose at z=-217.5cm. The bistatic RCS is plotted at $\theta=60^\circ$ for varying azimuth ϕ_s , for a plane wave incident at $\phi_i=90^\circ$ and $\theta_i=60^\circ$ (frequency $f=600\text{MHz}$, $N=11019$ unknowns).

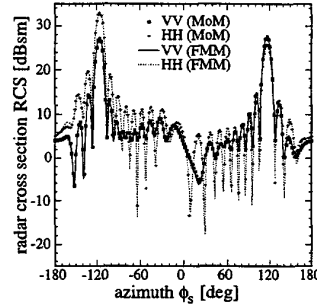


Fig. 3a RCS of a closed rectangular box with size $L_x \times L_y \times L_z = 12 \times 2 \times 2.5\text{m}^3$ situated 50cm above Yuma soil with 10% water. The co-polarized bistatic RCS (VV and HH) is plotted for varying azimuth angle ϕ_s at $\theta_i=80^\circ$ (i.e., 10° from grazing), for a plane wave incident at $\phi_i=60^\circ$ and $\theta_i=60^\circ$ (frequency is $f=150\text{MHz}$, 3776 triangles, leading to $N=5664$ unknowns).

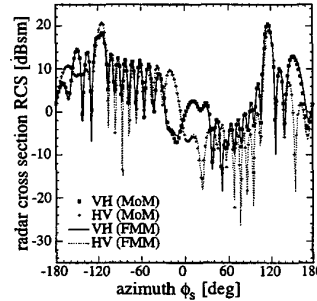


Fig. 3b Same as Fig. 3a, but plotting cross-polarized RCS (VH and HV).